Nuclear Engineering and Technology 55 (2023) 278–284

Contents lists available at ScienceDirect

Nuclear Engineering and Technology

journal homepage: www.elsevier.com/locate/net

Original Article

Physical characterization and radiation shielding features of B_2O_3–As_2O_3 glass ceramic

Mohamed Y. Hanfi [a, b, *], Ahmed K. Sakr [b, c], A.M. Ismail [b], Bahig M. Atia [b], Mohammed S. Alqahtani [d, e], K.A. Mahmoud [a, b]

[a] Ural Federal University, Ekaterinburg, 620002, Russia
[b] Nuclear Materials Authority, P.O. Box 530, El Maadi, Cairo, Egypt
[c] Department of Civil and Environmental Engineering, Wayne State University, 5050 Anthony Wayne Drive, Detroit, MI 48202, USA
[d] Radiological Sciences Department, College of Applied Medical Sciences, King Khalid University, Abha, 61421, Saudi Arabia
[e] BioImaging Unit, Space Research Centre, University of Leicester, Michael Atiyah Building, Leicester, LE1 7RH, UK

ARTICLE INFO

Article history:
Received 22 April 2022
Received in revised form
18 August 2022
Accepted 5 September 2022
Available online 9 September 2022

Keywords:
Glass-ceramic
Shielding features
Structure
MCNP
Melting

ABSTRACT

The synthetic B_2O_3–As_2O_3 glass ceramic are prepared to investigate the physical properties and the radiation shielding capabilities with the variation of concentration of the As_2O_3 with 10, 20, 30, and 40%, respectively. XRD analyses are performed on the fabricated glass–ceramic and depicted the improvement of crystallinity by adding As_2O_3. The radiation shielding properties are studied for the B_2O_3–As_2O_3 glass ceramic. The values of linear attenuation coefficient (LAC) are varied with the variation of incident photon gamma energy (23.1–103 keV). The LAC values enhanced from 12.19 cm^{-1}–37.75 cm^{-1} by raising the As_2O_3 concentration from 10 to 40 mol% at low gamma energy (23.1 keV) for BAs10 and BAs40, respectively. Among the shielding parameters, the half–value layer, transmission factor, and radiation protection efficiency are estimated. Furthermore, the fabricated samples of glass ceramic have low manufacturing costs and good shielding features compared to the previous work. It can be concluded the B_2O_3–As_2O_3 glass ceramic is appropriate to apply in X-ray or low-energy gamma-ray shielding applications.

1. Introduction

Nuclear energy is being used in a variety of industries, including energy production, military equipment, medicine, and agriculture. Workers in these fields, meanwhile, are at significant risk of exposure to radiation as a result of these technologies [38]. Acute radiation syndrome, which can result in worker death owing to the hematological subsyndrome caused by radiation damaging bone marrow tissue, can be caused by gamma radiation, a form of high-energy radiation [1–4]. One of many research groups' concealed aims during the last decade has been the demand for materials that may serve a dual role [5,6]. Nevertheless, these approaches have limitations, such as the fact that concrete is opaque, susceptible to cracking, immobile, and the water content of various samples can vary. Furthermore, lead (Pb) is a harmful material, thus, it is eschewed as much as thinkable for environmental reasons [7–9].

Nonetheless, protecting materials can be developed to attenuate γ–radiation over a considerable range of energies, and materials with appropriate high densities can be chosen depending on this [10,11]. Glasses and glass ceramic can be applied as both transparent and radiation-blocking materials [12,13]. Because of their numerous benefits, including ease of manufacture, cleanliness, clarity, light transparency, and portability, glasses, and glass ceramic have begun to garner considerable interest in this industry [3]. A mixture of two or more components is frequently used to make glasses. The glass and glass ceramic composition are determined by the application they will be employed. Glass ceramics can be clear to opaque because they include crystalline phases and, as a result, grain structure. Glass ceramics can vary from very crystalline to having a significant glassy phase [14,15]. Glass formers and modifiers can thus be used to change the features of glasses associated with physical and structural needs [16].

Glass formers are the fundamental structural component of the glass, hence high-density glass formers are essential for producing

* Corresponding author. Ural Federal University, Ekaterinburg, 620002, Russia.
E-mail addresses: mokhamed.khanfi@urfu.ru (M.Y. Hanfi), akhchemist@gmail.com (A.K. Sakr).

https://doi.org/10.1016/j.net.2022.09.006

an efficient shield. Glass can be formed using a variety of glass formers, including B_2O_3, TeO_2, SiO_2, P_2O_3, and GeO_2 [17,18]. The physical properties of the glasses, such as radiation shielding, can be enhanced by having metal oxides in precise ratios to their matrix [19–21]. The linear attenuation coefficient factor (LAC) is the most effective physical parameter for evaluating the capabilities of materials as radiation shielding instruments [22–27]. Monte Carlo codes can be used to evaluate the LAC. Based on the LAC, the other shielding parameters like half–value layer ($\Delta_{0.5}$), transmission factor (TF), and radiation protection efficiency (RPE) are estimated. The current study's major goal is to look into the structural, physical, and gamma–ray shielding capabilities of the manufactured (50-x) B_2O_3–x As_2O_3 glass-ceramics.

2. Materials and methods

2.1. Preparation of fabricated glass–ceramic

In the present study, the elastic properties of glassy samples with a chemical composition (50–x) B_2O_3–x As_2O_3 where x = 10, 20, 30, and 40 mol% were investigated. The replacement of B_2O_3 with As_2O_3 significantly affects the physical characteristics of the glass network. Pure chemical reagents of B_2O_3 and As_2O_3 were supplied by Merck Co., Germany. The studied samples were synthesized through the traditional melting technique. Pre-calculated masses of used chemicals were weighted using an electric balance with uncertainty of ± 0.001 mg and melted in platinum crucibles at a temperature of 1000 °C for 2 h. Bubble-free samples were obtained after melt swirling at constant time intervals to ensure reproducibility of the method. The molten was molded and the samples were annealed under an annealing temperature of 320 °C. The obtained glass–ceramic samples that were developed were given the following names:

BAs10 = BAs10: $40B_2O_3$–$10As_2O_3$
BAs20 = BAs20: $30B_2O_3$–$20As_2O_3$
BAs30 = BAs30: $20B_2O_3$–$30As_2O_3$
BAs40 = BAs40: $10B_2O_3$–$40As_2O_3$

2.2. Structural characterization

An X-ray diffraction system was employed to explore the structural behavior of the synthesized glasses ceramic using the Malvern Panalytical Empyrean device model, (2020) (Netherlands) using. Cu–target tube and Ni filter at 40 kV and 30 mA, Continuous scan type and 0.03 Step Size [°2Theta]. Samples were recorded in the range of 10–65°. Each sample weighed around 200 mg of a powder pounded by hand in an agate mortar (powder size was around 1.0 μm).

2.3. Shielding capacity

The mean track length (MTL) of the gamma photon inside the synthetic glass-ceramics was computed utilizing the Monte Carlo N-Particle transport code. Fig. 1 depicts the system's geometry, which is comprised of several cards. The first card (source card) gives information on the radioactive applied source (kind of emitted radiation) that is located at the (0, 0, 0) axis, such as its direction, position, energy, and photon distribution probability. The applied gamma sources had an energy interval (23.1–103 keV) along the Z-axis. Incident gamma rays were collimated via slits 1.0 cm in diameter in the collimator. The gamma rays were captured and subsequently impacted with the glass-ceramics sample. The second card, dubbed the material card, contains information about glass-ceramics samples (see Table 1).

The gamma rays generated by the source will pass through the glass-ceramics material on their way to the detector (F4 tally are selected to expect the mean flux per unit cell for the detector). The Monte Carlo code defined the cross-sectional data pertaining to the sources ENDF/B-VI.8. The NPS card has 106 histories on it [28].

The linear attenuation coefficient (LAC) was used to compute the material's radiation attenuation ability, which can be estimated using the equation below (1) [29]:

$$LAC = \left(\frac{1}{x}\right)\ln\left(\frac{I_0}{I}\right) \quad (1)$$

The calculation depends on the incident intensity of gamma

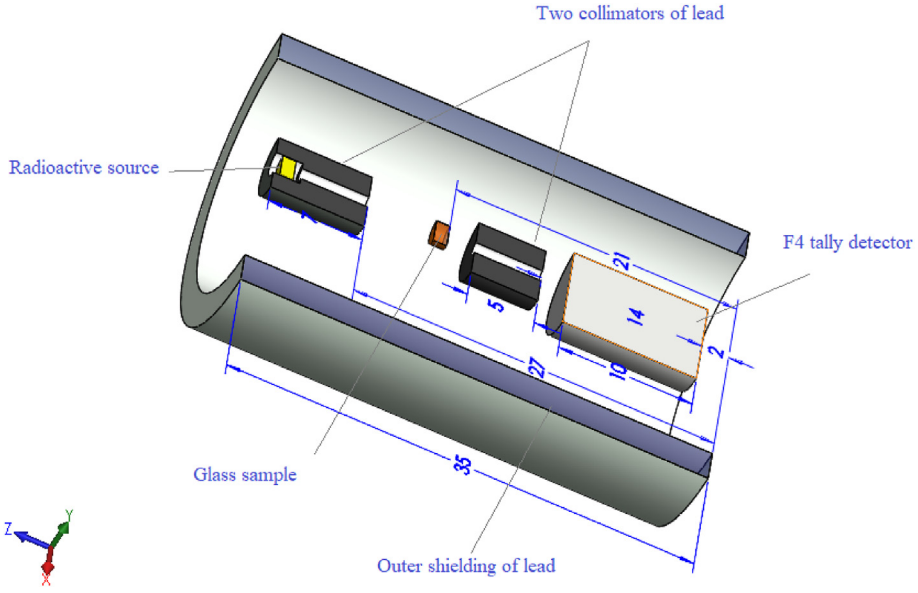

Fig. 1. The MCNP simulation geometry configuration.

radiation (I_o) and the transmitted intensity of gamma radiation (I) through the thickness of glass ceramic (x, cm).

The glass-ceramic thickness that may cut incident gamma radiation in half is referred to as the shielding parameter ($\Delta_{0.5}$). The $\Delta_{0.5}$ can be calculated utilizing the formula below (2) [30,37].

$$\Delta_{0.5} = \frac{ln(2)}{LAC(cm^{-1})} \quad (2)$$

The transmission factor (TF) is a formula that can be used to predict the coefficient of gamma photon transport through a specific thickness of glass-ceramics (3) [31].

$$TF(\%) = \frac{I}{I_o} = \exp(-\mu x) \quad (3)$$

The radiation protection efficiency (RPE) can be determined via the following equation (4):

$$RPE = \left(1 - \frac{I}{I_o}\right) \times 100\% \quad (4)$$

3. Results and discussion

3.1. XRD

The thermal heat treatment processes of boric acid at 330 °C led to not completely crystalized Boron oxide (B_2O_3). The XRD pattern of boron oxide (B_2O_3), shows its characteristic peaks of d−spacing 3.21, 6.07, and 2.94 Å at °2Theta 27.77°, 14.58°, and 30.32°, respectively, which are in agreement with PDF−2 Card No. (06−297) which crystallized in the Cubic system (Fig. 2a). The heat treatment by adding well-crystalized agents such as arsenic oxide (As_2O_3) leads to more crystalized specific composition. XRD pattern of added As_2O_3 shows its characteristic sharp peaks of d−spacing 3.18, 6.35, and 1.95 Å at 2Theta 27.98°, 13.93°, and 46.42°, respectively, which match PDF−2 Card No. (72−1333) (Fig. 2b).

After the addition of variable arsenic oxide (As_2O_3) content, a relative improvement in crystallinity has been achieved; it is noted a decrease in the proportion of the amorphous content and growth of crystalline phases (Fig. 2c,d,e,f). The comparisons among different concentrations of arsenic oxide (As_2O_3) indicate an increase in intensity (Fig. 2g). The relationship between intensity and arsenic oxide content for the most intense peak at 2Theta of 27.98° reveals a clear improvement in the crystallinity, as presented in (Fig. 2h) [32−34].

3.2. Radiation Shielding

Fig. 3 reveals the variance of the LAC of the glass-ceramics (BAs) with the incident gamma photon energy. The interactions of arriving gamma photons with the material compositions of the BAs glass-ceramics will be among the three main interactions; Photoelectric effect (PE), Compton Scattering (CS), and Pair production (PP). It can be explained as follow: First, it can be noticed that the LAC has high values at the low gamma photon energy. This is

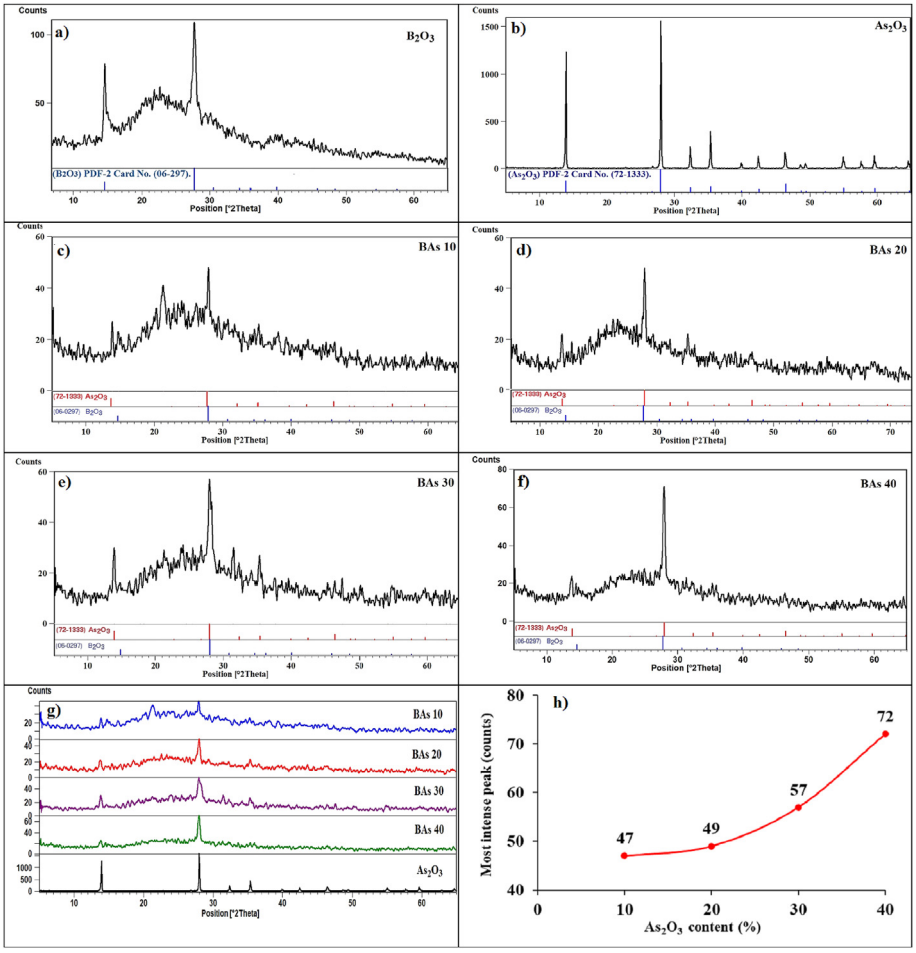

Fig. 2. XRD pattern of the BAS glass ceramics.

Table 1
The chemical composition of the studied glass-ceramics samples.

Formations	Compositions (mol %)		Density	MW
	As_2O_3	B_2O_3	(g/cm^3)	(g/mol)
BAs10	10	90	2.01	82.442
BAs 20	20	80	2.17	95.264
BAs 30	30	70	2.23	108.086
BAs 40	40	60	2.43	120.908

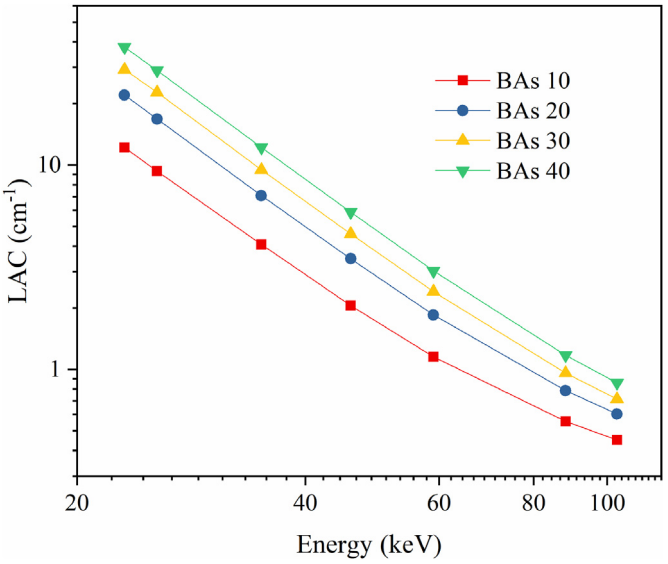

Fig. 3. The variation of linear attenuation coefficient (LAC) with the incident gamma photon energy of the glass ceramic.

generated due to the type of interaction between the gamma photons and the glass-ceramic material, where the dominant at the low energy is the photoelectric effect (PE). According to the PE interaction, the glass-ceramic material has a good ability to attenuate the incident gamma photons. In this case, the cross-section of PE is directly proportional to the inverse of incident photon energy ($\sigma_{PE} \propto 1/E^3$) and directly proportional to the atomic number ($\sigma_{PE} \propto Z^{7/2}$), respectively. The highest LAC values are detected at the low energy (E = 23.2 keV), the range of LAC values varied between 12.19 and 37.75 cm^{-1} for BAs10 and BAs40, respectively. Second, it can be observed that the PE interactions will be disappeared at the increment of photon energy, where the LAC values fall progressively owing to the predominant CS interactions with the glass-ceramic material. Obviously, the incident gamma photons interacted with the materials, and the part of gamma photons attenuated inside the glass-ceramic and the rest of the photons are scattered, therefore, the LAC values are diminished. Moreover, the CS cross-section is proportional to the effective atomic number Z_{eff} ($\sigma_{CS} \propto Z_{eff}$). Consequently, the lowest LAC values varied from 0.45 to 0.85 cm^{-1} at the high photon energy (E = 103 keV) for BAs 10 and BAs 40, respectively.

Besides the effectiveness of photon energy on the LAC values, the chemical composition of BAs glass-ceramics also affected the LAC values. The present glass-ceramics BAs include two sub-compositions As_2O_3 and $B_2O_3$with various concentrations. Fig. 3 displays that at the identified photon energies, the LAC affected the glass-ceramic compositions. This means the compactness between the molecules of the glass-ceramic material increase with the increment of As_2O_3 concentration and the decrement of B_2O_3 concentration. Therefore, it is clarified that at the low concentration of As_2O_3 (10%) the compactness between the glass material molecules is weak. Thus, the capability of glass-ceramic to attenuate the incident gamma photons seemed low. The minimum values of LAC are registered in the glass-ceramic (BAs 10 = $10As_2O_3$+$90B_2O_3$) which alternated from 0.45 to 12.19 cm^{-1}. While the increase of As_2O_3 (20–40%) concentration in the chemical composition of the investigated glass-ceramics lead to the raising the compactness between the molecules of the material and the capability of the glass-ceramic increased enough to attenuate the incident gamma photons. The maximum LAC values are predicted in the glass ceramic with high As_2O_3 concentrations (BAs 40 = $40As_2O_3$+$60B_2O_3$), which changed between 0.85 and 37.75 cm^{-1}.

Fig. 4 exhibits the variation of $\Delta_{0.5}$ values that affected the incident gamma photon energy (E, MeV) and the composition of glass ceramic ((50-x)B_2O_3+xAs_2O_3). It is observed that the $\Delta_{0.5}$ values increased with the elevation of gamma photon energy (Fig. 4). The lowest simulated $\Delta_{0.5}$ values are balanced at the low gamma-photon energy (E = 23.1 keV) and reduced from 0.05 to 0.01 cm for BAs 10 and BAs 40, respectively. The increment of incident gamma-photon energy leads to an increase slowly in the simulated $\Delta_{0.5}$ values and the highest values are achieved at the high gamma-photon energy (E = 103 keV), which diminishes from 1.5 to 0.8 cm for BAs 10 and BAs 40, respectively. It was noticed that the CS interaction is prevalent in the chosen energy range (23.1–103 keV), thus $\Delta_{0.5} \propto E$. Subsequently, $\Delta_{0.5}$ was discovered to rise with gamma photon energy.

The effect of As_2O_3 in the chemical composition (50−x) B_2O_3+xAs_2O_3) on $\Delta_{0.5}$ values is observed as described in Fig. 4. It is seen that the addition of As_2O_3 content progressively diminished $\Delta_{0.5}$. At certain gamma energies, the highest values of $\Delta_{0.5}$ are detected in the C1 (ρ = 2.01 g/cm^3), where it varied from 0.05 to 1.5 cm. While the lowest values in the BAs 40 (ρ = 2.43 g/cm^3) are changed from 0.01 to 0.8 cm. With the insertion of As_2O_3 concentration into the glass-ceramic, the density and molecular weight of the examined glass-ceramic lessened. Furthermore, the Z_{eff} of the glass-ceramic reduces, which guides to a reduction to the LAC and the increment to the $\Delta_{0.5}$ of the glass-ceramic. Therefore, it means the BAs 40 glass-ceramic with minimum values of $\Delta_{0.5}$ can be employed as the radiation shielding applications at various incident gamma energy (23.1–103 keV).

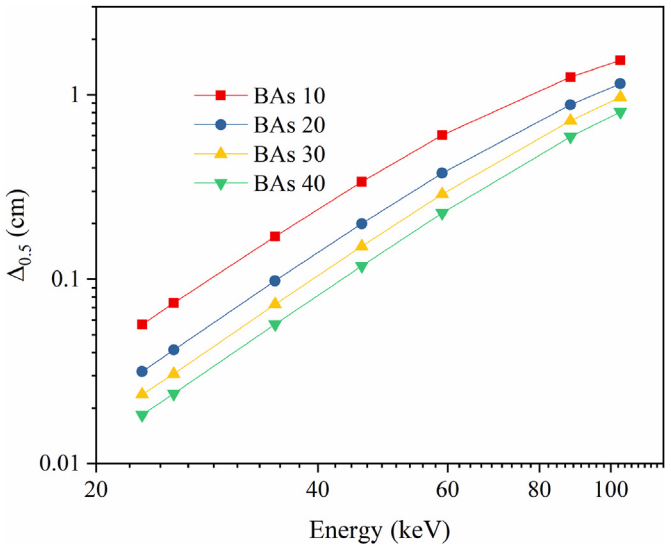

Fig. 4. The variation of half−value layer ($\Delta_{0.5}$) with the incident gamma photon energy of the glass ceramic.

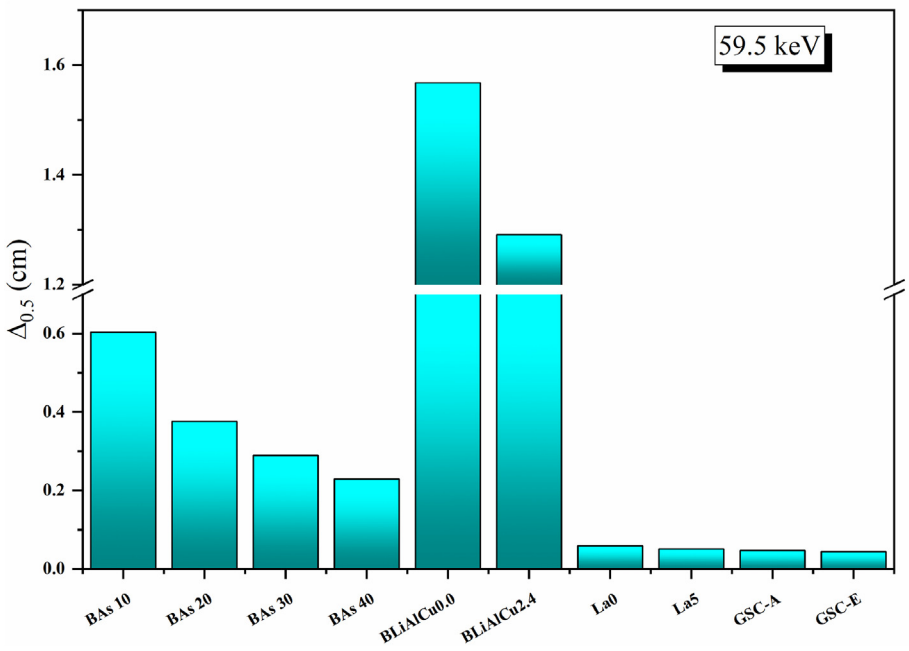

Fig. 5. Comparison between the $\Delta_{0.5}$ of the fabricated glasses and some previously published glass-ceramics.

The $\Delta_{0.5}$ values corresponding to the fabricated glass-ceramics were compared to the previous works of literature in order to validate the fabricated samples. Fig. 5 presents that the $\Delta_{0.5}$ values at gamma-ray energy of 0.662 MeV for the fabricated glass-ceramic samples are 0.603, 0.376, 0.289, and 0.229 cm for samples BAs 10, BAs 20, BAs 30, and BAs 40 respectively. These $\Delta_{0.5}$ values are lower than that reported for glass ceramics BLiAlCu0.0 and BLiAlCu2.4 with $\Delta_{0.5}$ values of 1.567 and 1.291 cm [35]. On the other hand, the fabricated samples $\Delta_{0.5}$ are thicker than that reported for glasses ceramic La0, La5, GSC-A, and GSC-E with $\Delta_{0.5}$ values of 0.059, 0.051, 0.047, 0.044 cm, respectively [36]. Although the fabricated glass-ceramic has thicker $\Delta_{0.5}$ values than the earlierly mentioned samples, they have an advantage related to the manufacturing cost. Regarding the manufacturing cost, the fabricated glass-ceramics samples have a lower fabrication cost compared to samples La0, La5, GSC−A, and GSC−E. The mentioned samples La0, La5, GSC−A, and GSC−E contain TeO_2, La_2O_3, GeS_2, and CSCL compounds that are relatively expensive compared to the fabricated glass-ceramic compounds B_2O_3 and As_2O_3.

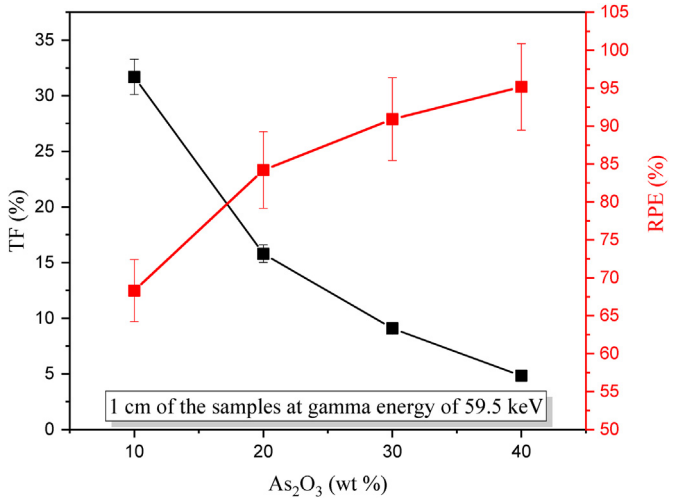

Fig. 6. Effect of As_2O_3 incrementation on the TF and RPE of the fabricated glass-ceramic samples.

Fig. 6 illustrates the role of As_2O_3 on variation of the transmission factor (TF, %) and radiation protection efficiency (RPE, %). The TF is a measure of the number of transmitted gamma photons to the total number of incident photons (I/I_o). In contrast, the RPE is a measure of the number of absorbed photons inside the shielding material to the total number of the incident photons ($I_{absorbed}/I_o$) where $I + I_{absorbed} = I_o$. Fig. 4 illustrates that the incrementation of As_2O_3 with density to the fabricated glass-ceramic samples increases the ρ values of the fabricated samples. The ρ values enhanced from 2.01 to 2.43 g/cm^3, raising the As_2O_3 incrementation ratio between 10 and 40 wt%. The early mentioned increase in the sample ρ values was followed by an enhancement of the LAC values of the fabricated samples. This affected the number of transmitted photons I from the fabricated samples where the I values decreased compared to the total number of the incident photons. Thus, the Transmission value (I/I_o) decreased as a result of raising the As_2O_3 incrementation concentration. In contrast, the number of absorbed photons ($I_{absorbed}$) increased with raising the ρ and μ values of the fabricated samples. Thus, the net ratio of ($I_{absorbed}/I_o$) increased associated with an increase in the RPE values. For example, at a gamma photon energy of 59.5 keV, the TF values decreased between 31.694, 15.799, 9.089, and 4.829%. On the other hand, the RPE for the fabricated samples enhanced between 68.306, 84.201, 90.911, and 95.171%, raising the As_2O_3 incrementation concentration between 10, 20, 30, and 40 wt%, respectively at 59.5 keV.

The fabricated glass-ceramic thickness is also an important factor that can control the values of I and $I_{absorbed}$, where increasing the glass thickness causes an increase in the distance that the photons transpose inside the fabricated samples. Thus, the values of $I_{absorbed}$ increased compared to the I values. As a result, the net values of (I/I_o) decreased associated with an increase in the net value of ($I_{absorbed}/I_o$) when the fabricated glass-ceramic samples' thickness increased from 0.25 to 2.0 cm. Fig. 7 illustrated that for sample BAs 10 (for example) the TF values reduced from 75.032% to 10.045% while the RPE enhanced from 24.968 to 89.955% with

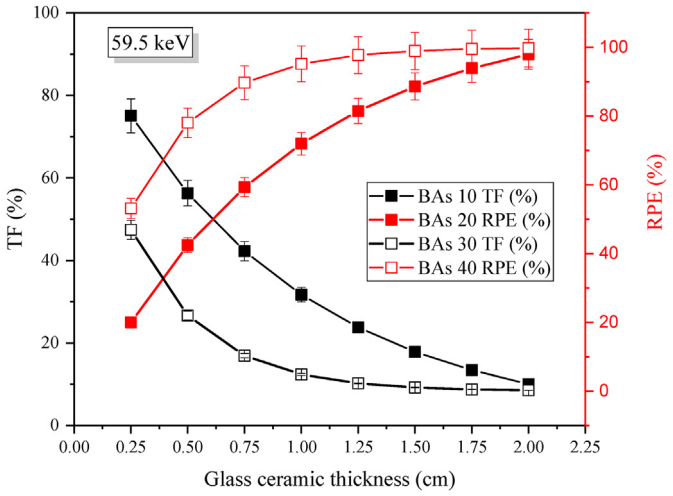

Fig. 7. Effect of the fabricated glass-ceramic thickness on the TF and RPE.

growing the sample thickness between 0.25 cm and 2.0 cm at a gamma photon energy of 59.5 keV. At the same mentioned energy, the TF values decreased from 21.974 to 0.233% while the RPE increased from 53.123% to 99.767%, raising the sample BAs 40's thickness from 0.25 cm to 2.0 cm, respectively.

4. Conclusion

A series of four glass-ceramic samples were fabricated as a mixture of binary compounds B_2O_3 and As_2O_3 under a melting temperature of 1000 °C. The phase and structure of the fabricated glasses-ceramic samples were affirmed using the XRD, where a relative improvement in crystallinity has been achieved by adding As_2O_3. Moreover, the fabricated glass-ceramic shielding capacity for low gamma energy photons was evaluated and examined using the Monte Carlo simulation. The highest LAC values were achieved in the current study at gamma energy photon of 23.1 keV, where the μ values enhanced from 12.195 cm^{-1}–37.757 cm^{-1}. In contrast, the lowest LAC values varied between 0.451 cm^{-1} and 0.859 cm^{-1}, raising the As_2O_3 concentration between 10 and 40 wt%, respectively. The enhancement of LAC values was reflected in the other shielding parameters where the $\Delta_{0.5}$ values for the fabricated glass-ceramic samples were reduced by raising the As_2O_3 concentration in the fabricated glass-ceramics. For example, the $\Delta_{0.5}$ at gamma energy photon of 59.5 keV is 0.603, 0.376, 0.289, and 0.229 cm for glass-ceramic sample BAs 10, BAs 20, BAs 30, and BAs 40, respectively. Furthermore, the TF was reduced while the RPE was enhanced by increasing the As_2O_3 concentration in the fabricated samples. The fabricated glass-ceramic samples showed good shielding properties and manufacturing costs compared to some previously published similar glass-ceramic materials. Thus, the fabricated sample can be used in X-ray or low-energy gamma-ray shielding applications.

Declaration of competing interest

The authors declare that they have no known competing financial interests or personal relationships that could have appeared to influence the work reported in this paper.

Acknowledgment

The authors extend their appreciation to the Deanship of Scientific Research at King Khalid University (KKU) for funding this work through the Research Group Program Under the Grant Number (R.G.P.2/248/43).

References

[1] Y. Al-Hadeethi, M.I. Sayyed, Y.S. Rammah, Fabrication, optical, structural and gamma radiation shielding characterizations of GeO2-PbO-Al2O3–CaO glasses, Ceram. Int. 46 (2020) 2055–2062, https://doi.org/10.1016/j.ceramint.2019.09.185.
[2] K.M. Kaky, M.I. Sayyed, A. Khammas, A. Kumar, E. Şakar, A.H. Abdalsalam, B. Cevîz Şakar, B. Alim, M.H.A. Mhareb, Theoretical and experimental validation gamma shielding properties of B2O3-ZnO-MgO-Bi2O3 glass system, Mater. Chem. Phys. (2020) 242, https://doi.org/10.1016/j.matchemphys.2019.122504.
[3] M.I. Sayyed, F. Akman, M.R. KaÇal, A. Kumar, Radiation protective qualities of some selected lead and bismuth salts in the wide gamma energy region, Nucl. Eng. Technol. 51 (2019) 860–866, https://doi.org/10.1016/j.net.2018.12.018.
[4] K.A. Mahmoud, M.I. Sayyed, A.M.S. Alhuthali, M.Y. Hanfi, The effect of CuO additive on the mechanical and radiation shielding features of Li2B4O7-Pb2O3 glass system, Bol. la Soc. Esp. Ceram. y Vidr. (2020) 3–11, https://doi.org/10.1016/j.bsecv.2020.11.005.
[5] M. Rahimi, M. Zahedifar, R. Azimirad, A. Faeghinia, Luminescence and scintillation properties of Eu2+ doped CaF2 glass ceramics for radiation spectroscopy, J. Lumin. 221 (2020), 117040, https://doi.org/10.1016/j.jlumin.2020.117040.
[6] M.J. Dejneka, The luminescence and structure of novel transparent oxyfluoride glass-ceramics, J. Alloys Compd. 239 (1998) 149–155, https://doi.org/10.1016/s0022-3093(98)00731-5.
[7] M. Środa, S. Świontek, D. Fraś, Effect of Ga2O3 on the structure and properties of TeO2–GeO2 glass doped with Pr3+, J. Non. Cryst. Solids (2019), 119699.
[8] O. Agar, M.I. Sayyed, H.O. Tekin, K.M. Kaky, S.O. Baki, I. Kityk, An investigation on shielding properties of BaO, MoO3 and P2O5 based glasses using MCNPX code, Results Phys. 12 (2019) 629–634, https://doi.org/10.1016/j.rinp.2018.12.003.
[9] A.H. Abdalsalam, M.I. Sayyed, T.A. Hussein, E. Şakar, M.H.A. Mhareb, B.C. Şakar, B. Alim, K.M. Kaky, A study of gamma attenuation property of UHMWPE/Bi 2 O 3 nanocomposites, Chem. Phys. 523 (2019) 92–98, https://doi.org/10.1016/j.chemphys.2019.04.013.
[10] M. Cai, B. Zhou, Y. Tian, J. Zhou, S. Xu, J. Zhang, Broadband mid-infrared 2.8 Mm emission in Ho3+/Yb3+-codoped germanate glasses, J. Lumin. 171 (2016) 143–148, https://doi.org/10.1016/j.jlumin.2015.11.016.
[11] C.L. Medrano-Pesqueira, D.A. Rodríguez-Carvajal, Structural properties of poly-crystals embedded in glassy matrix of the ternary system CdO-TeO2-GeO2, J. Non. Cryst. Solids 475 (2017) 15–24, https://doi.org/10.1016/j.jnoncrysol.2017.07.024.
[12] S.N. Nazrin, M.K. Halimah, F.D. Muhammad, J.S. Yip, L. Hasnimulyati, M.F. Faznny, M.A. Hazlin, I. Zaitizila, The effect of erbium oxide in physical and structural properties of zinc tellurite glass system, J. Non. Cryst. Solids 490 (2018) 35–43, https://doi.org/10.1016/j.jnoncrysol.2018.03.017.
[13] S.A. Tijani, S.M. Kamal, Y. Al-Hadeethi, M. Arib, M.A. Hussein, S. Wageh, L.A. Dim, Radiation shielding properties of transparent erbium zinc tellurite glass system determined at medical diagnostic energies, J. Alloys Compd. 741 (2018) 293–299, https://doi.org/10.1016/j.jallcom.2018.01.109.
[14] M. Kamislioglu, E.E. Altunsoy Guclu, H.O. Tekin, Comparative evaluation of nuclear radiation shielding properties of XTeO2 + (100–x)Li2O glass system, Appl. Phys. A Mater. Sci. Process. 126 (2020), https://doi.org/10.1007/s00339-020-3284-3.
[15] S.H. Alazoumi, H.A.A. Sidek, M.K. Halimah, K.A. Matori, M.H.M. Zaid, A.A. Abdulbaset, Synthesis and elastic properties of ternary ZnO-PbO-TeO2 glasses, Chalcogenide Lett. 14 (2017) 303–320.
[16] J.E. Stanworth, Physical Properties of Glass, The Clarendon Press, Oxford, 1950.
[17] K.A. Matori, M.I. Sayyed, H.A.A. Sidek, M.H.M. Zaid, V.P. Singh, Comprehensive study on physical, elastic and shielding properties of lead zinc phosphate glasses, J. Non. Cryst. Solids 457 (2017) 97–103, https://doi.org/10.1016/j.jnoncrysol.2016.11.029.
[18] M. Çelikbilek, A.E. Ersundu, S. Aydin, Preparation and characterization of TeO2-WO3-Li 2O glasses, J. Non. Cryst. Solids 378 (2013) 247–253, https://doi.org/10.1016/j.jnoncrysol.2013.07.020.
[19] K.A. Mahmoud, F.I. El-Agwany, Y.S. Rammah, O.L. Tashlykov, Gamma ray shielding capacity and build up factors of CdO doped lithium borate glasses: theoretical and simulation study, J. Non. Cryst. Solids 541 (2020), 120110, https://doi.org/10.1016/j.jnoncrysol.2020.120110.
[20] Y.S. Rammah, K.A. Mahmoud, M.I. Sayyed, F.I. El-Agawany, R. El-Mallawany, Novel vanadyl lead-phosphate glasses: P2O5–PbO–ZnO[sbnd]Na2O–V2O5: synthesis, optical, physical and gamma photon attenuation properties, J. Non. Cryst. Solids 534 (2020), 119944, https://doi.org/10.1016/j.jnoncrysol.2020.119944.
[21] P. Vishwanath, Singh, M.E. Medhat, S.P. S, Comparative studies on shielding properties of some steel alloys using Geant4, MCNP, WinXCOM and experimental results, Radiat. Phys. Chem. 106 (2015) 255–260, https://doi.org/10.1016/j.radphyschem.2014.07.002.
[22] K.A. Naseer, K. Marimuthu, K.A. Mahmoud, M.I. Sayyed, Impact of Bi2O3 modifier concentration on barium–zincborate glasses: physical, structural,

elastic, and radiation-shielding properties, Eur. Phys. J. Plus (2021) 136, https://doi.org/10.1140/epjp/s13360-020-01056-6.
[23] G. Kilic, F.I.E. Agawany, B.O. Ilik, K.A. Mahmoud, E. Ilik, Y.S. Rammah, Ta2O5 reinforced Bi2O3–TeO2–ZnO glasses: fabrication, physical, structural characterization, and radiation shielding efficacy, Opt. Mater. (Amst). 112 (2021), 110757, https://doi.org/10.1016/j.optmat.2020.110757.
[24] Q. Chen, K.A. Naseer, K. Marimuthu, P.S. Kumar, B. Miao, K.A. Mahmoud, M.I. Sayyed, Influence of modifier oxide on the structural and radiation shielding features of Sm3+-doped calcium telluro-fluoroborate glass systems, J. Aust. Ceram. Soc. 57 (2021) 275–286, https://doi.org/10.1007/s41779-020-00531-8.
[25] S. Arivazhagan, K.A. Naseer, K.A. Mahmoud, K.V. Arun Kumar, N.K. Libeesh, M.I. Sayyed, M.S. Alqahtani, E.S. Yousef, M.U. Khandaker, Gamma-ray protection capacity evaluation and satellite data based mapping for the limestone, charnockite, and gneiss rocks in the sirugudi taluk of the dindigul district, India, Radiat. Phys. Chem. 196 (2022), 110108, https://doi.org/10.1016/j.radphyschem.2022.110108.
[26] N.K. Libeesh, K.A. Naseer, K.A. Mahmoud, M.I. Sayyed, S. Arivazhagan, M.S. Alqahtani, E.S. Yousef, M.U. Khandaker, Applicability of the multispectral remote sensing on determining the natural rock complexes distribution and their evaluability on the radiation protection applications, Radiat. Phys. Chem. 193 (2022), 110004, https://doi.org/10.1016/j.radphyschem.2022.110004.
[27] N.K. Libeesh, K.A. Naseer, S. Arivazhagan, A.F.A. El-Rehim, G. ALMisned, H.O. Tekin, Characterization of ultramafic–alkaline–carbonatite complex for radiation shielding competencies: an experimental and Monte Carlo study with lithological mapping, Ore Geol. Rev. 142 (2022), 104735, https://doi.org/10.1016/j.oregeorev.2022.104735.
[28] H.A. Al-Yousef, M. Alotiby, M.Y. Hanfi, B.M. Alotaibi, K.A. Mahmoud, M.I. Sayyed, Y. Al-Hadeethi, Effect of the Fe2O3 addition on the elastic and gamma-ray shielding features of bismuth sodium-borate glass system, J. Mater. Sci. Mater. Electron. 32 (2021) 6942–6954, https://doi.org/10.1007/s10854-021-05400-z.
[29] M.H.A. Mhareb, Physical, optical and shielding features of Li2O–B2O3–MgO–Er2O3 glasses Co-doped of Sm2O3, Appl. Phys. A Mater. Sci. Process. 126 (2020) 1–8, https://doi.org/10.1007/s00339-019-3262-9.
[30] S. Yesmin, B. Sonker Barua, M. Uddin Khandaker, M. Tareque Chowdhury, M. Kamal, M.A. Rashid, M.M.H. Miah, D.A. Bradley, Investigation of ionizing radiation shielding effectiveness of decorative building materials used in Bangladeshi dwellings, Radiat. Phys. Chem. 140 (2017) 98–102, https://doi.org/10.1016/j.radphyschem.2016.11.017.
[31] D.I. Tishkevich, T.I. Zubar, A.L. Zhaludkevich,, I.U. Razanau, T.N. Vershinina, A.A. Bondaruk, E.K. Zheleznova, M. Dong, M.Y. Hanfi, M.I. Sayyed, M.V. Silibin, S.V. Trukhanov, A.V. Trukhanov, Isostatic hot pressed W–Cu composites with nanosized grain boundaries: microstructure, structure and radiation shielding eefficiency against gamma rays, Nanomaterials 12 (2022) 1–15, https://doi.org/10.3390/nano12101642.
[32] K.A. Naseer, P. Karthikeyan, S. Arunkumar, P. Suthanthirakumar, K. Marimuthu, Enhanced Luminescence Properties of Er3+/Yb3+ Doped Zinc Tellurofluoroborate Glasses for 1.5 Mm Optical Amplification, 2020, 030237.
[33] K.A. Naseer, K. Marimuthu, M.S. Al-Buriahi, A. Alalawi, H.O. Tekin, Influence of Bi2O3 concentration on barium-telluro-borate glasses: physical, structural and radiation-shielding properties, Ceram. Int. 47 (2021) 329–340, https://doi.org/10.1016/j.ceramint.2020.08.138.
[34] K.A. Naseer, G. Sathiyapriya, K. Marimuthu, T. Piotrowski, M.S. Alqahtani, E.S. Yousef, Optical, elastic, and neutron shielding studies of Nb2O5 varied Dy3+ doped barium-borate glasses, Optik (Stuttg). 251 (2022), 168436, https://doi.org/10.1016/j.ijleo.2021.168436.
[35] B. Albarzan, M.Y. Hanfi, A.H. Almuqrin, M.I. Sayyed, H.M. Alsafi, K.A. Mahmoud, The influence of titanium dioxide on silicate-based glasses: an evaluation of the mechanical and radiation shielding properties, Materials 14 (2021), 3414, https://doi.org/10.3390/ma14123414.
[36] F.I. El-Agawany, K.A. Mahmoud, E. Kavaz, R. El-Mallawany, Y.S. Rammah, Evaluation of nuclear radiation shielding competence for ternary Ge–Sb–S chalcogenide glasses, Appl. Phys. A Mater. Sci. Process. 126 (2020) 1–11, https://doi.org/10.1007/s00339-020-3426-7.
[37] K.A. Mahmoud, O.L. Tashlykov, A.F. El Wakil, H.M.H. Zakaly, I.E. El Aassy, Investigation of radiation shielding properties for some building materials reinforced by basalt powder, AIP Conf. Proc. 2174 (2019), 020036, https://doi.org/10.1063/1.5134187.
[38] I. Gaafar, M. Hanfi, L.S. El-Ahll, I. Zeidan, Assessment of radiation hazards from phosphate rocks, Sibaiya area, central eastern desert, Egypt, Appl. Radiat. Isot. 173 (2021), 109734, https://doi.org/10.1016/j.apradiso.2021.109734.